9

Artificially Rendered Cutaneous Cues for a New Generation of Haptic Displays

Enzo Pasquale Scilingo[1], Matteo Bianchi[1], Nicola Vanello[2], Valentina Hartwig[1], Luigi Landini[2], and Antonio Bicchi[1]

[1] Interdepartmental Research Center "E. Piaggio", University of Pisa, via Diotisalvi, 2, 56126, Pisa, Italy
e.scilingo@ing.unipi.it

[2] Department of Information Engineering, University of Pisa, via G. Caruso, 16, 56122, Pisa, Italy

Summary. In this chapter we report on two architectures of haptic devices able to reproduce variable softness and elicit tactile sensations. Both solutions aim at addressing more effectively cutaneous channels. The first device is comprised of a tactile flow-based display coupled with a commercial kinesthetic interface. The second device is based on a pin array configuration in order to stimulate locally the fingertips and induce the illusion of different shapes or moving objects.

9.1 Introduction

Tactual sensory experience includes two distinct perceptual channels: kinesthetic information referring to the sensation of positions, velocities, forces and constraints arising from the muscle spindles and tendons. Force feedback haptic interfaces mostly rely on kinesthetic senses by presenting force-position control to create the illusion of contact with rigid or compliant surfaces. The cutaneous class of sensations arises through direct contact with the skin surface. When designing haptic displays, both of these channels should be elicited [1]. While it is quite simple to provide kinesthetic information, cutaneous information elicitation is still not sufficient. There are several attempts in literature to convey cutaneous information, e.g. by means of shape and/or vibration feedback, or by providing thermal data [2–4]. Here, we propose two technological solutions. The first one is based on the mechanical coupling of two displays while the second solution implies using a pin array display for locally deforming the fingertip skin.

The first display relies on a conjecture, first proposed by [5, 6], based on surrogating detailed tactile information for softness discrimination with infor-

mation on the rate of spread of the contact area between the finger and the object as the contact force increases. This conjecture relies on the paradigm that a large part of haptic information necessary to discriminate softness of objects by touch is contained in the law that relates resultant contact force to the overall area of contact, or in other terms in the rate by which the contact area spreads over the finger surface as the finger is increasingly pressed on the object. Authors called this relationship Contact Area Spread Rate (CASR). Such a conjecture does not pretend to minimize the importance of other relevant aspects of tactile information, such as, e.g., shape of the contact zone or pressure distribution in the contact area, but it only suggests that the CASR information might increase tactile perception. For the sake of citation, next works [7] presented a softness display based on the control of fingertip contact area, although it was not able to display the dynamic change of the contact area and did not have enough spatial resolution.

Starting from a good resemblance between the growing rate of the contact area between the finger pad and an object during a tactile indentation task and the convergence or divergence of the vision field in time to contact task, we formulated a more general paradigm than CASR. In particular, the divergence from focus of expansion of optic flow represents the expansion of iso-brightness contours. The area delimited by a closed iso-brightness contour grows with motion over time likewise the growth of the contact area in the tactile domain. This analogy led us to define a new conjecture, inspired to optic flow, which we called *tactile flow*. Several works supported this conjecture [8,9]. Hereinafter, we will refer to Tactile Flow (TF) display in place of CASR display.

The TF display, which mainly addresses cutaneous channels [10], is mechanically coupled with a commercial device, the Delta Haptic Device (DHD) by Force Dimension [11], which instead provides mostly kinesthetic information. In this chapter we will experimentally verify if this combination is able to constructively join the advantages of each device improving the overall performance. Indeed, the TF device is able to provide careful force/area and force displacement relationships, but due to mechanical constraints, these two behaviors are intimately related. On the other hand, the DHD can reliably provide force/displacement relationships, but it is not able to reproduce force/area relationships. Combining the two devices, therefore, we can independently control force/area and force/displacement relationships, thus extending the range of materials which can be reproduced. In addition, there are some materials which have the same force/displacement, but different force/area relationships (this latter, indeed, strongly depends on the geometry) and only an independent control of the two behaviors can replicate a similar rheology.

The second device is based on the concept of locally mechanically stimulating the fingertip skin in order to evoke different cutaneous sensations. The idea behind this device is to design a simple architecture which can be easily adapted to be used in fMRI environments. Generally, mechanical tactile displays utilize actuated components to actively deform the user skin via

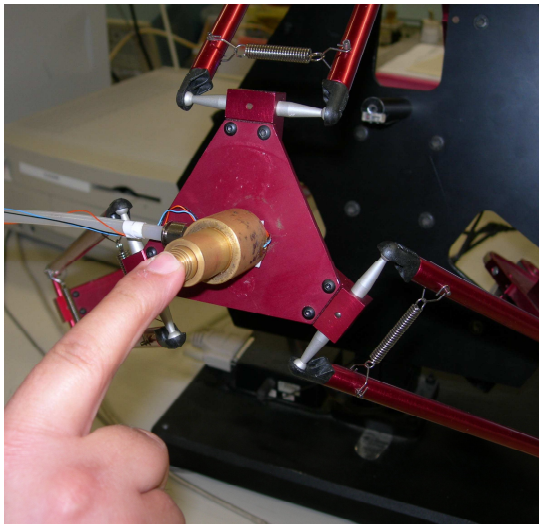

Fig. 9.1. Picture showing the haptic system.

pressure, stretch or other means, in order to induce controlled touch sensations. They can be further classified by their method of stimulation into vibration, lateral displacement (skin stretch) and skin indentation. Vibration displays present shape information via activating patterns of spatially configured transducers at high temporal frequencies of operation. These elements tend to be much smaller than the vibrotactile transducers, for example, pins or wires driven by solenoids or piezoelectric actuators [12]. Devices for lateral displacement present information through spatiotemporal patterns of skin stretch [13] and [14]. Tactile displays for skin indentation present distributed cues by inducing pressure on the skin via a number of moving elements. They have received the most attention for virtual environment applications as they offer the most significant potential to represent the fingertip deformations that occur in touch interaction with everyday objects. In literature there are several devices based on raised static pin patterns, as well as vibrotactile displays. The former find wide application in the development of embossed raised characters for visually impaired people, e.g. Braille display. Vibrotactile displays consist of a single element stimulator that is used to encode information in temporal parameters of the vibration signal. Parameters that can potentially be employed include frequency, amplitude, waveform, duration and rhythm [15]. Stimulation can be generated by various means including, but not limited to, solenoids, voice coils or rotation of an inertia by a motor. Most people make use of vibrotactile technology within mobile phones, as a non-audio-based indicator of an incoming call or text message. Vibrotactile information has also found widespread acceptance within the video gaming community as an inexpensive means of providing touch feedback in hand held controllers. Here we

propose a mechanical display able to stimulate the fingertip with a pattern of pins and we investigate how tactile sensation changes with the frequency by which pins go up and down.

9.2 The Holistic TF-based Haptic System

The haptic system here proposed is comprised of a TF display [5] placed on the top of the Delta Haptic Device (DHD) (see Fig. 9.1. The TF display is a pneumatic device consisting of a set of cylinders of different radii in telescopic arrangement (see right side of Fig. 9.2). A regulated air pressure is inflated inside the display and acts on the cylinders so as to provide a simulated compliance which can be perceived by the operator when pushing with their forefinger against the top of the display. The schematic view of the TF display is shown on the left side of Fig. 9.2. A proportional Hall sensor placed at

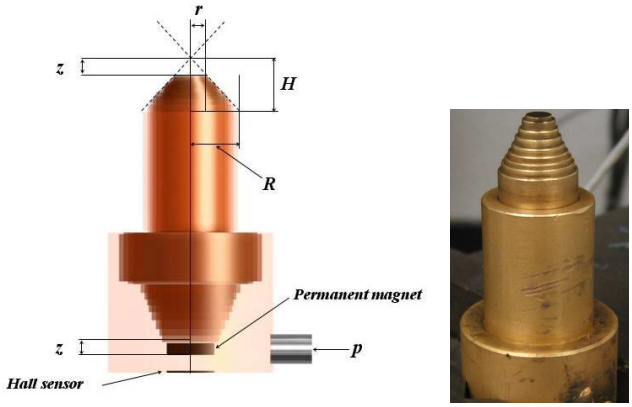

Fig. 9.2. Schematic view (left) and picture (right) of the TF display.

the bottom of the inner chamber allows measuring the displacement z of the cylinders when the subject pushes against them, while a servo pneumatic actuator regulates the chamber pressure according to the desired CASR profile to replicate. The Delta Haptic Device is a commercial interface, widely used by the haptic research community. It is a high performance haptic device and has 6 degrees of freedom: 3 translations from the parallel Delta structure and 3 rotations from a wrist module. Unlike other haptic mechanisms having either limited force capability or small workspace, the DHD is capable of providing large forces (up to 25N) over a large volume (30 cm diameter, 30 cm length). In addition, because of its design and its base-mounted actuators, the device offers high stiffness, decoupled translation and rotation, as well

as very low inertia. The haptic system exploits both performance of the two devices, joining the high fidelity and quality of tactile information of the TF display to the large workspace and high stiffness of the DHD.

9.3 Theoretical Justification

The initial contact of a mechanical interaction between two bodies may occur at a point in case of spherical geometry or along a line in case of cylindrical bodies [16]. Let us focus on spherical geometry. Applying a slight load the area around the initial contact point begins deforming. In such a way the mechanical interaction takes place on a finite smaller area than bodies dimensions. Contact theory predicts the shape of contact area and its behavior with time and with increasing load. Moreover, it allows identifying stress and strain components in both bodies within and outside the loaded area.

When two spherical solids come into contact, the initial contact occurs at a single point which spreads over a circular area. According to the Hertz theory [16] the pressure exerted onto a generic circular area having radius r within the contact area between two solids of revolution is

$$p(r) = \frac{p_0}{a}\sqrt{(a^2 - r^2)}, \qquad r \leq a$$

where a is the radius of the circular contact area and p_0 is the pressure at the origin. The total pressure is

$$P = \int_0^a p(r) 2\pi r dr = \frac{2}{3} p_0 \pi a^2.$$

Introducing the equivalent quantity

$$\frac{1}{E^*} = \frac{1 - \nu_1^2}{E_1} + \frac{1 - \nu_2^2}{E_2}$$

where E_1, E_2, ν_1 and ν_2 are the Young modulus and Poisson ratio for the two bodies coming into contact, respectively, we can obtain obtain the radius of contact area:

$$a = \frac{\pi p_0 R}{2E^*} \tag{9.1}$$

From this latter equation, it is worthwhile noting that Young modulus, contact area and curvature radius are strictly and intimately correlated. Young modulus relates the applied force (stress) with the induced displacement (strain). Eq. (9.1) says that if two bodies are constitutively made of the same material, hence they have the same Young modulus, i.e. the same force/displacement, but different curvature radii, then they have different force/area behavior.

In order to replicate the rheology of these materials, it is necessary to implement an independent control of force/displacement and force/area. The TF

display is able to replicate force/area behaviors with high reliability from a perceptual point of view, but it does not allow to implement two independent profiles of force/area and force/displacement. Indeed, when an external force is applied on the device it returns a reaction force given by $F = PA(z)$, where P is the pressure inflated into the inner chamber of the display and $A(z)$ is the contact area. This latter, however, is strictly related to the normal displacement by the bijective relationship $A(z) = \pi \frac{z^2 R^2}{H^2}$, where z is the normal displacement, R is the cylinder radius and H is the height of the cone (see Fig. 9.2). Therefore, when a force/area profile is set, force/displacement is indirectly obtained. On the other hand, DHD is a haptic interface which enables to reliably replicate force/displacement curves, but it does not allow to provide force/area behavior. By coupling the two devices, it is possible to control independently force/area and force/displacement, joining synergistically the two performance.

9.4 Hardware Equipment: Modeling and Identification

In this section, we modeled the TF device in order to analytically characterize it in terms of force/area relationships parameterized with by pressure. Afterwards, these curves were experimentally validated inflating inside the TF device progressive constant pressures and measuring the force/area profile at each pressure level.

9.4.1 Theoretical model of TF display

If we assume the system lossless, while the probing finger pushes with a constant force F against the top of the display, this latter exerts an equal and opposite reaction at the equilibrium position in agreement with the virtual work principle:

$$F\delta z = -p\delta V \Rightarrow F = -p\frac{\delta V}{\delta z}, \tag{9.2}$$

where δz and δV are respectively the virtual displacement along the z axis, and the virtual variation of the volume V of the TF display. The variation of the inner volume of the TF display is given by

$$\delta V = -\pi \frac{z^3 R^2}{3H^2},$$

in which $H = 0.01$ m is the maximum height, and $R = 0.0065$ m is the radius calculated at the basis of the CASR display. According to (9.2), we easily obtain the analytical model for the display

$$F = p\pi \frac{z^2 R^2}{H^2} = pA. \tag{9.3}$$

9.4.2 Experimental model of TF display

The analytical model previously calculated has been experimentally assessed using the hardware setup shown in Fig. 9.3. The TF display was submitted to indentation tests at different pressures by means of a compressional indentor driven by an electromagnetic mini-shaker. The actuator, made by Bruel & Kjear, is a linear current step motor mini-shaker type, capable of applying a maximum displacement of 10 mm in axial direction. The indentor is a metallic cylinder of 1.5 cm in diameter and 10 cm in length. The indentor is equipped with a magnetic linear transducer, Vit KD 2300/6C by KAMAN Science Corporation, used to measure the applied axial displacement and with a load cell sensor, ELH-TC15/100 by Entran, able to detect forces up to ± 50 N.

An external electronic driver is used to activate the indentor and acquire force-position signals from the sensors.

A data acquisition PCI card with one analog output channel and two analog input channels, is used to gather signals and sent them to a PC. A dedicated software was implemented in Matlab/Simulink environment to control in feedback and in real-time the displacement of the indentor and to record and plot the signals.

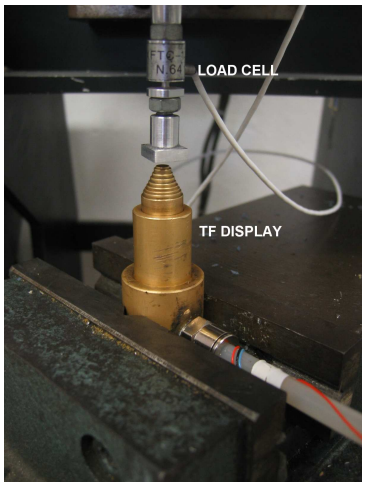

Fig. 9.3. Experimental setup used for identifying the TF model.

9.4.3 Identification assessment

The TF display was characterized in terms of force versus axial displacement at different values of pressure. Keeping the pressure constant, as the shaker pushes onto the TF display the outputs from both force and position sensor

are recorded. The pressure inside the display is maintained constant as the shaker pushes by an internal control of a servovalve, Proportion-Air's QB series, employed for this purpose. The experimental curves were compared with the theoretical ones. In Fig. 9.4 three experimental force/area curves at three different values of pressure were compared with the corresponding theoretical ones. Results show a satisfactory agreement between three any TF force/displacement curves and those theoretically calculated at the same pressures. This supports the hypothesis that the air loss inside the TF display can be considered negligible.

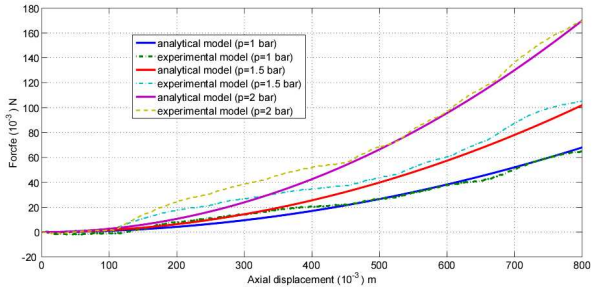

Fig. 9.4. Force/Displacement response of the TF display compared with the analytical model at three different levels of pressure, by way of illustration.

9.5 Experimental Session

An experimental protocol was applied to two sphere-shaped viscoelastic specimens, M_1 and M_2, approximately homogeneous and with different curvature radii, where both force-area and force-displacement curves are acquired. Fig. 9.5 shows the experimental setup used to acquire force/area curves. The same hardware setup used for characterizing the TF display was additionally equipped with a dedicated area sensor. The specimen was positioned onto a transparent plexiglass surface whereunder a web camera was placed. As the indentor pushes against the specimen the web cam captures a snapshot of the surface flattened against the plexiglass. In order to enhance contours of contact area a thin white paper behaving as optical filter was placed between the specimen and the plexiglass. In addition to force/area, also the indentation depth is detected by a magnetic position sensor. In Fig. 9.6 two snapshots of the contact area were captured on the same specimen at two different level of indenting force are shown. The experimental force/area curves acquired by the hardware setup previously described as well as the corresponding mathematical interpolated curves are reported in Fig. 9.7 for the two specimens. A quadratic interpolation provided best fitting.

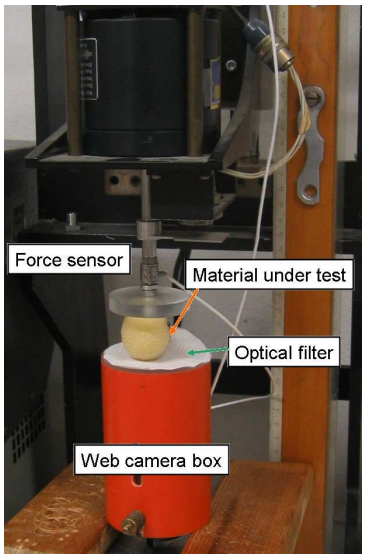

Fig. 9.5. Experimental setup used for identifying force/area curve of the specimens.

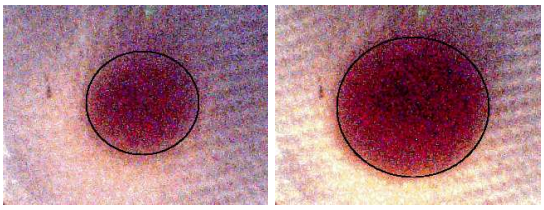

Fig. 9.6. Two different snapshots of the contact area captured on the same specimen having radius $R = 1.3cm$ at two level of force.

Two spherical specimens of the same material M_1, having radii $R = 1.1$ cm and $R = 1.3$ cm, respectively, and two specimens of the material M_2 having radii $R = 1.4$ cm and $R = 1.7$ cm were characterized in terms of force/area and force/displacement. Experimental curves of force/area were interpolated and as expected from the Hertz theory best fitting was obtained by a quadratic interpolation. These equation were used in the control law. Here we report, by way of illustration, the interpolated equation for the specimen of radius $R = 1.1$ cm of the material M_1:

$$F(A)|_{(M_1,R=1.1)} = 1.4A^2 + 0.33A + 0.55. \tag{9.4}$$

Fig. 9.7 shows all the four experimental force/area relationships along with the interpolated ones, for the material M1 and M2, respectively on the left and right. An analogous procedure was done for force/displacement identification.

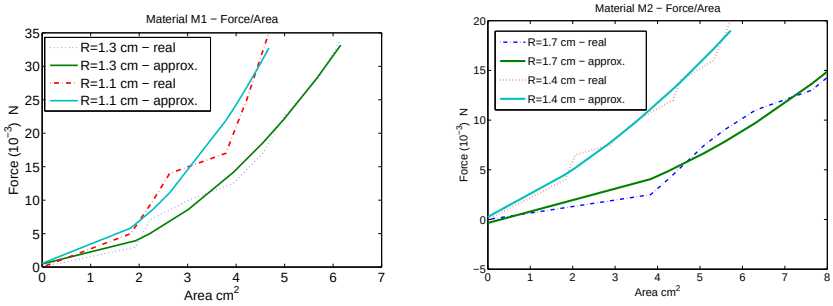

Fig. 9.7. Experimental force/area relationships and interpolated curves for two sphere-shaped specimens of the same material M_1 having radius ($R = 1.3cm$ and $R = 1.1cm$.) on the left side and M_2 having radius ($R = 1.7cm$ and $R = 1.4cm$) on the right side

Results are reported in Fig. 9.8 left and right side. As can be seen, these curves are mathematically approximated by a linear interpolation.

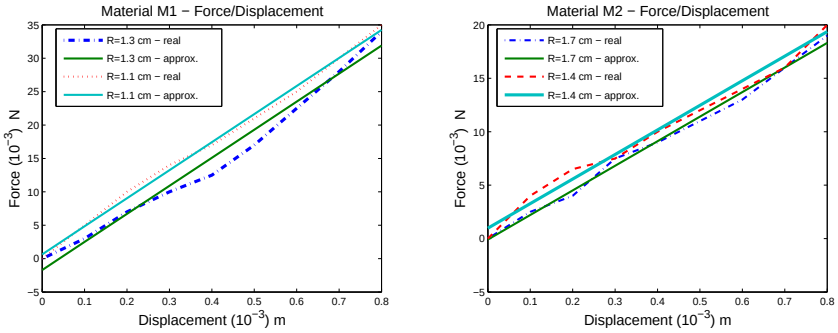

Fig. 9.8. Force/Displacement relationships and approximations of spherical specimen M_1 having different radius ($R = 1.3cm$ and $R = 1.1cm$) on the left side and M_2 having different radius ($R = 1.7cm$ and $R = 1.4cm$) on the right side.

For the sake of brevity, here we report the equation of the interpolated curve for the specimen of material M_2 with radius $R = 1.4cm$

$$F(z)|_{(M_2,R=1.4)} = 23z + 0.97. \tag{9.5}$$

It is worthwhile noting that the slope of the interpolated curves for the same material is the same, in agreement with the theory that same materials, though with different geometry, have the same Young modulus, hence roughly the same force/displacement curves.

9.5.1 Control strategy

The proposed, integrated haptic system allows replicating any force/area and force/displacement relationships, thanks to the possibility of independently controlling the displacement z_D of the DHD in addition to the air pressure p inflated inside the CASR device. If we denote, indeed, z_C and z_D the displacements of the CASR and of the DHD respectively, both force/area and force/displacement relationships can be mapped by the independent set of controls p and $z_D = z_m - z_C$, where z_m is the material displacement to replicate.

Let us suppose to replicate, e.g., the material M_1, neglecting the terms of zero and first order in the force/area equation as well as the intercept in the straight-line equation of force/displacement:

$$\begin{cases} F_m = \alpha_m A_m^2, \\ z_m = \beta_m F_m. \end{cases} \tag{9.6}$$

The force/area relationship should be reproduced by the CASR device, whose force/area characteristic is reported in (9.3). Imposing the same force and area of the material to replicate, we get

$$p = \alpha_m A_m. \tag{9.7}$$

In order to track the force/displacement behavior, we should set

$$z_m = z_C + z_D, \tag{9.8}$$

where z_C is read by the position sensor placed inside the CASR display and is analytically given by the combination of (9.3) and (9.7).

Coupling the two devices mechanically in series, we have $F_C = F_D$ which in turn should be equal to F_m. This force is the input of DHD, while the output z_D is controlled in feedback so that $z_D = z_m - z_C$, which can be expressed as

$$z_D = z_m - z_C = \beta_m F_m - z_C = \beta_m p \frac{\pi R^2}{H^2} z_C^2 - z_C. \tag{9.9}$$

9.6 Experimental Results

In order to assess the performance of the control strategy, we replicated the behavior of the materials M_1 and M_2, previously identified. Pushing on the haptic system with a desired force profile, the control law responded in terms of area and displacement in agreement with the analytical model of materials previously identified. Output from displacement and area sensors of the haptic system were compared with the analytical desired trajectories and we reported experimental results in Figs. 9.9 and 9.10. As it can be seen, this new

architecture is able to successfully track the theoretical curves with negligible errors. In addition to good tracking performance, the combined system is also able to provide increased haptic feeling and further psychophysical experiments aiming at assessing that are planned to be performed. This confidence is supported by results from previous works [5]. Indeed, in the new combined system here proposed, cutaneous information is mostly provided by the CASR display which was already shown to better discriminate softness with respect to a purely kinaesthetic display but additionally kinaesthetic information is increasingly enhanced by DHD performance, in terms of accuracy and reliability.

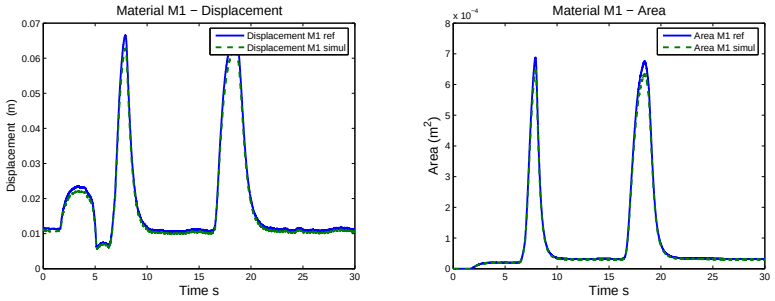

Fig. 9.9. Tracking of the displacement (on the left side) and area (on the right side) of M_1 by the haptic system. Continuous line represents the response of the model of the material to an external force, while dashed line is the tracking output of the system.

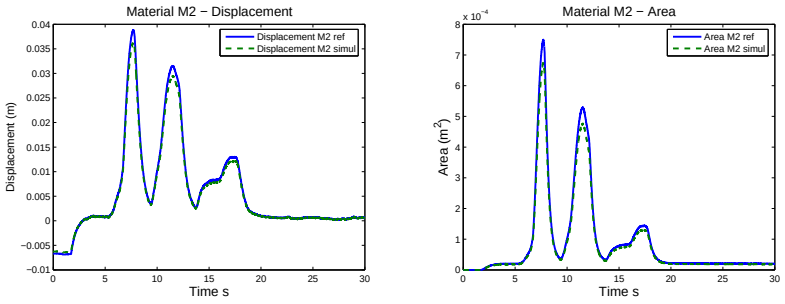

Fig. 9.10. Tracking of the displacement (on the left side) and area (on the right side) of M_2 by the haptic system. Continuous line represents the response of the model of the material to an external force, while dashed line is the tracking output of the system.

9.7 The Pin-based Mechanical Stimulator

One approach to render spatial aspects of the tactile sense is the use of pin arrays, i.e. a fingertip sized array of small pins that can be moved individually. Movement can be modulated in frequency up to achieve a vibratory stimulation. Here we propose a very simple haptic display which is based on a 4x4 pin array configuration. This architecture was thought to be fMRI compatible. This haptic display is comprised of a 4x4 pin array, which is moved by 16 servo motors. Each motor is controlled independently using a graphic interface in LabView. It is possible to change the frequency of the control signal hence the stimulator pin velocity. Pins are constituted of 1 mm diameter metal bars with a round rubber tip to avoid any finger injuries and are spaced 2 mm apart. Sixteen servo motors are used to move the pins up and down, in vertical direction: these motors have a plastic case and are controlled by a pulse signal. The rotation angle of the motor axes is correlated to the pulse width, so that, by changing the parameters of the control signal, it is possible to vary the movement of the pin bar. All the motors are fixed on a dedicated PVC structure with a perforated ceil to support the pin array (see Fig. 9.11). Motor control is obtained using a DAQ National Instrument acquisition card

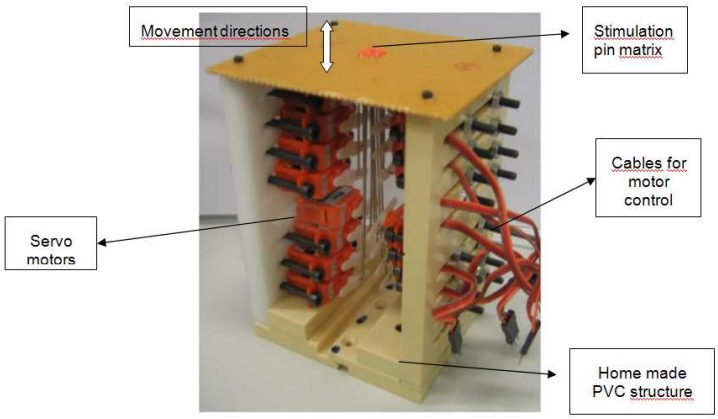

Fig. 9.11. Mechanical structure of the device.

and a notebook with LabView software. Using a graphic interface it is possible to choose the parameters of the control signals of each motor: duty cycle, frequency, pulse width, signal length and phase. The amplitude of all control signals is 1 V. Through the graphic interface the user can choose the pin to act. Each of the 16 pins can be actuated independently or combined.

9.7.1 Experimental tests

Preliminary tests on the new haptic device were performed in order to assess performance. Two experimental sessions were set out. The first one aimed at investigating how frequency affects the capability of localizing the mechanical stimulating point. The second experiment focused on a preliminary study for verifying whether the device is able to induce illusionary movements and therefore to replicate the paradigm of tactile flow by stimulating the pins in the manner of a progressive wave.

Spatial localization

The first test focused on the identification and localization of a tactile stimulus obtained with one pin. Subjects were asked to place their right forefinger on the stimulation array and lean their wrists on a support to limit hand movements. Only one of the 16 pins was actuated using different frequencies (3, 5, 10 Hz): the subject was asked to indicate the number of the moving pin according to the scheme shown in Fig. 9.12, left side. The test involved 5

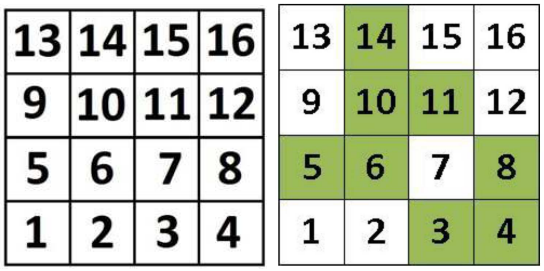

Fig. 9.12. Order of pins in stimulation matrix.

stimulation sessions: for each session only one pin was moved for 10 seconds with three different stimulation frequencies (3, 5 10 Hz) using a pulse train with 5 pulse of 1.5 ms and five pulses of 2 ms. At the end of each stimulation session subjects were asked to indicate the pin activated reporting the number according to the matrix scheme. Due to technical limitations only 8 pins out of 16 were used and more specifically the numbers indicated in Fig. 9.12, right side, but subjects were in the dark about that. The different pins were activated with different frequencies according to a random protocol. Eight subjects participated in the test (5 male, 3 female, age 25-30 years, right handed). Fig. 9.13 shows the results of the described test in terms of correct localization percentages, for each stimulation frequency used. It is worthwhile noting that most of exact responses (62.5%) were obtained at the highest frequency (10 Hz) and the number of exact responses increases as the

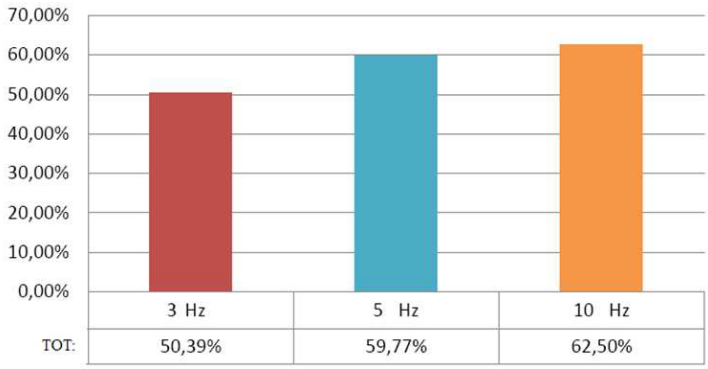

Fig. 9.13. Correct localization percentage.

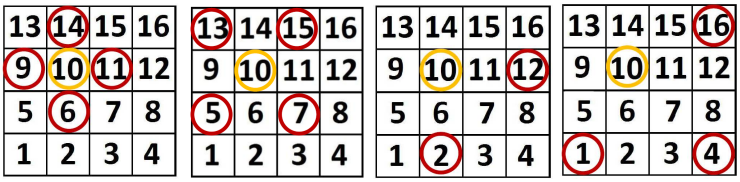

Fig. 9.14. Types of error in localizing the stimulating point, from A to D reading from left to right.

stimulation frequency grows. This can be interpreted as a wider involvement of SAI mechanoreceptors (Merkel corpuscles) and RA afferents (Meissner's corpuscles) which are most sensitive to this dynamic mechanical stimulus at that frequency. Moreover, they are the most numerous receptor types with fine spatial sensitivity and are best at the fingertips. In addition, the analysis of the results indicates that, independently of the stimulation frequency used, the best localized pin is the number 4. This would imply that subjects are more able to localize stimulating point at the edges than central points. In order to complete the study, we defined four types of error:

Error A: The subject indicates a pin right adjacent to the activated one on the same row or the same column. For example: pin stimulated=10, pin indicated by the subject= 9 or 11 or 14 or 6;

Error B: The subject indicates a pin close to the activated one but not on the same row or same column. For example: pin stimulated= 10, pin indicated to the subject= 13 or 15 or 5 or 7;

Error C: The subject indicates a pin on the same row or the same column of the activated pin but not close to this one. For example: pin stimulated= 10, pin indicated to the subject= 2 or 12;

Error D: The subject indicates a pin not on the same row or the same column of the activated pin and not close to this one. For example: pin stimulated= 10, pin indicated to the subject= 16 or 1 or 4;

Fig. 9.14 shows in graphical form the four types of errors. Fig. 9.15 shows the percentages of the four error types at different stimulation frequencies. For all the frequencies used the most frequently occurred error is the A type. This means that, even if subjects did not identify correctly the stimulation point, she/he can approximately localize the right stimulation position in the most of cases.

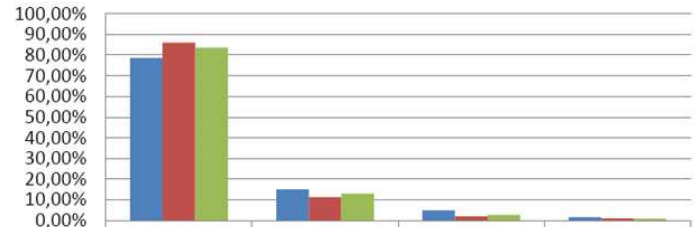

	A	B	C	D
3 Hz	78,57%	15,08%	4,76%	1,59%
5 Hz	85,98%	11,21%	1,87%	0,93%
10 Hz	83,62%	12,93%	2,59%	0,86%

Fig. 9.15. Percentage of errors made by the subjects.

Apparent movement of pins

A very preliminary experimental protocol was arranged in order to verify if the device is able to induce dynamic stimuli, i.e. moving dots. Only one single row is used and pins are driven with variable delay in order to obtain different stimulation conditions. More specifically, three different configurations are envisaged: wave traveling rightwards, wave traveling leftwards and no wave. Rightwards wave (see third column in Fig. 9.16) means that the peak is moving spatially over time rightwards; analogously leftwards wave is schematically represented in the first column. No wave means that there is no moving peak, but the central pin is alternating with the two lateral ones. A group of 21 subjects volunteered to participate in the experiment, 8 males and 134 females, age comprised between 21 and 24, all right-handed. The experiment consist in two trials of six stimulations, and each configuration is presented randomly twice. The aim was to investigate the capability of recognizing the movement of the virtual wave and possibly the direction. Two types of analysis were carried out. The first one aimed at assessing whether subjects are able to perceive

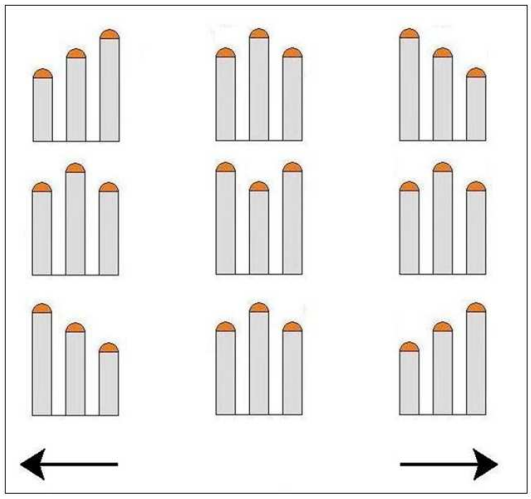

Fig. 9.16. Different stimulating waves.

a moving dot under the fingerpad. The second aimed at analyzing whether subjects that perceived the movement are also able to correctly identify the direction of motion. Results are reported in Fig. 9.17.

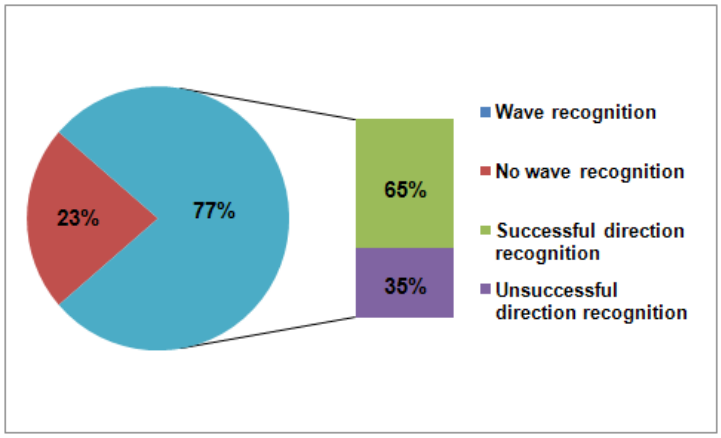

Fig. 9.17. 77% of subjects perceived a moving pin under the fingerpad and among these 65% identified correctly the direction.

9.8 Conclusion

In the first part of this chapter we proposed a new configuration of a haptic system comprised of two devices mechanically coupled in series. This new architecture allowed to implement an independent control of force/area and force displacement, extending the range of materials which can be replicated. After introducing the theoretical motivation we identified four specimens consisting of two materials, M_1 and M_2 each one of two different sizes. The two specimens having different geometry of the same material M_1 exhibit the same force/displacement, but different force/area. They can be replicated only by a device able to implement an independent control of the two relationships. The same is true of the material M_2. Experimental results showed that the newly proposed system is able to effectively track every curve of each material. The last part of the chapter was dedicated to evaluating performance of a pin array device. The idea behind was to verify if the device is able to reproduce simple shapes using several pins simultaneously and illusionary moving patterns. Finally, future work will address the compatibility of the new haptic device for fMRI based investigations of brain functions related to tactile tasks, in order to verify the hypothesis of the recruitment of different areas by changing stimulation parameters.

Acknowledgments

This work was partly supported by the ImmerSence project within the 6th Framework Programme of the European Union, FET - Presence Initiative, contract number IST-2006-027141, see also www.immersence.info.

References

1. Caldwell, D., Lawther, S., Wardle, A.: Multi-modal cutaneous tactile feedback. In: IEEE/RSJ International Conference on Intelligent Robots and Systems IROS, Osaka, Japan (1996) 465–472
2. Hayward, V., Astley, O., Cruz-Hernandez, M., Grant, D., Robles-De-La-Torre, G.: Haptic interfaces and devices. Sensor Review **24**(1) (2004) 16–29
3. Yano, H., Komine, K., Iwata, H.: Development of a high-resolution surface type haptic interface for rigidity distribution rendering. In: First World Haptics Conference, Pisa, Italy (2005) 465–472
4. Srinivasan, M.A., LaMotte, R.: Tactile discrimination of softness. Journal of Neurophysiology **73**(1) (1995) 88–101
5. Bicchi, A., De Rossi, D.E., Scilingo, E.: The role of the contact area spread rate in haptic discrimination of softness. IEEE Transactions on Robotics and Automation **16**(5) (2000) 496–504

6. Bicchi, A., Scilingo, E., Dente, D., Sgambelluri, N.: Tactile flow and haptic discrimination of softness. In Barth, F., Humphrey, J., Secomb, T., eds.: Multipoint interaction with real and virtual objects. Springer Tracts in Advanced Robotics (2005) 165–176
7. Fujita, K., Ohmori, H.: A new softness display interface by dynamic fingertip contact area control. In: 5th World Multiconference on Systemics, Cybernetics and Informatics,, Pisa, Italy (2001) 78–82
8. Bicchi, A., Scilingo, E., Ricciardi, E., Pietrini, P.: Tactile flow explains haptic counterparts of common visual illusions. Brain Res Bulletin **75**(6) (2008) 737–741
9. Ricciardi, E., Vanello, N., Sani, L., Gentili, C., Scilingo, E., Landini, L., Guazzelli, M., Bicchi, A., Haxby, J., Pietrini, P.: The effect of visual experience on the development of functional architecture in hMT+. Cerebral Cortex **17**(12) (2007) 2933–2939
10. Goldstein, E.: The cutaneous senses. Sensation and Perception **443** (2002) 329–355
11. : Delta haptic device. http://www.forcedimension.com (2011)
12. Summers, I., Chanter, C.: A broadband tactile array on the fingertip. The Journal of the Acoustical Society of America **112** (2002) 2118
13. Pasquero, J., Hayward, V.: Stress: A practical tactile display system with one millimeter spatial resolution and 700 hz refresh rate. In: Proc. Eurohaptics. Volume 2003., Citeseer (2003) 94–110
14. Caldwell, D., Tsagarakis, N., Giesler, C.: An integrated tactile/shear feedback array for stimulation of finger mechanoreceptor. In: Robotics and Automation, 1999. Proceedings. 1999 IEEE International Conference on. Volume 1., IEEE (1999) 287–292
15. Brewster, S., Brown, L.: Tactons: structured tactile messages for non-visual information display. In: Proceedings of the fifth conference on Australasian user interface-Volume 28, Australian Computer Society, Inc. (2004) 15–23
16. Johnson, K.: Contact mechanics. Cambridge University Press (1985)